

Self-supervision through Random Segments with Autoregressive Coding (RandSAC)

Tianyu Hua^{1,5}, Yonglong Tian², Sucheng Ren³, Hang Zhao⁴, Leonid Sigal^{1,5,6}

¹University of British Columbia ²Massachusetts Institute of Technology

³South China University of Technology ⁴Tsinghua University

⁵Vector Institute for AI ⁶Canada CIFAR AI Chair

Abstract. Inspired by the success of self-supervised autoregressive representation learning in natural language (GPT and its variants), and advances in recent visual architecture design with Vision Transformers (ViTs), in this paper, we explore the effects various design choices have on the success of applying such training strategies for *visual* feature learning. Specifically, we introduce a novel strategy that we call **Random Segments with Autoregressive Coding** (RandSAC). In RandSAC, we group patch representations (image tokens) into hierarchically arranged segments; within each segment, tokens are predicted in parallel, similar to BERT, while across segment predictions are sequential, similar to GPT. We illustrate that randomized serialization of the segments significantly improves the performance and results in distribution over spatially-long (across-segments) and -short (within-segment) predictions which are effective for feature learning. We illustrate the pertinence of these design choices and explore alternatives on a number of datasets (*e.g.*, CIFAR10, ImageNet). While our pre-training strategy works with vanilla Transformer, we also propose a conceptually simple, but highly effective, addition to the decoder that allows learnable skip-connections to encoder feature layers, which further improves the performance. Our final model¹, trained on ImageNet, achieves new state-of-the-art linear probing performance (68.3%) among comparative predictive self-supervised learning approaches.

Keywords: Vision Tranformer (ViT) feature learning, generative autoregressive pretraining, self-supervised learning

1 Introduction

Deep learning has powered enormous successes in Computer Vision and NLP over the past 10, or so, years. It has lead to significant improvements in object detection [42], segmentation [24], as well as higher-level cognition tasks (*e.g.*, Visual Question Answering [1], Visual Navigation [35], *etc.*). These successes have been enabled by both advances in parallel hardware (GPUs) and, perhaps more importantly, large-scale task-specific labeled datasets that allow supervised

¹ Code will be released at <https://github.com/PatrickHua/RandSAC>.

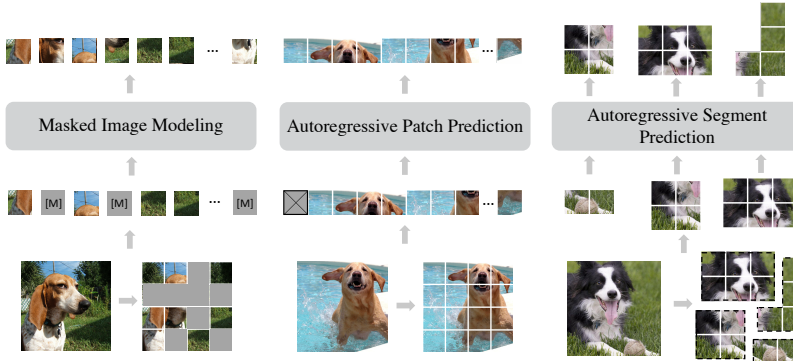


Fig. 1: **Randomized Autoregressive Segment Prediction.** Illustration of our autoregressive segment prediction framework (RandSAC) compared with other predictive frameworks. Left: BERT-style masked image modeling, where all masked patches are predicted in parallel. Middle: GPT-style autoregressive modeling which is trained to predict next pixel/patch in fixed raster-order. Source sequence is shifted one token to the right. Right: proposed RandSAC approach.

learning. This appetite for large data has, until very recently, stagnated progress, particularly in building general-purpose visual architectures.

These types of considerations date back to the early days of machine learning, and deep learning in particular, where it has long been postulated that unsupervised, or self-supervised, learning could allow learning of robust and general feature representations that can then be readily used (or fine-tuned) to target tasks. Early works in vision date back to CNN-based unsupervised learning (*e.g.*, using forms of denoising autoencoders [39, 50], colorization [61] or jigsaw puzzle [16, 36] proxy objectives). However, the success of such self-supervised pre-training was somewhat limited. In contrast, the success of similar self-supervised ideas in NLP has been much more dominant with GPT [3] and BERT [15] architectures, and their variants. These pre-training strategies now enable state-of-the-art, and in some cases human-level, performance on a wide array of natural language tasks.

Recent advances in vision architectures, such as Vision Transformers (ViT) [17, 31], which serialize visual 2d data, have opened an opportunity to apply similar large scale pre-training techniques in vision, with increasing successes. Self-supervised pre-training techniques with ViTs can be characterized into two broad categories: *contrastive* and *predictive*; as well as their combinations. In *contrastive* pre-training architectures are learned to be invariant to certain perturbations in data (*e.g.*, spatial shifts, color jitter) by forming positive and negative pairings of augmented data samples. This is a powerful technique, but requires designers to make assumptions about invariances that the architecture should learn. In addition, purely contrastive models tend to incorporate *center bias* [9, 8], which makes them less transferable for tasks such as segmentation where non-object centric regions need to be modeled. Alternatively, *predictive* models learn to predict elements of the scene, either in parallel by reconstructing masked regions/tokens [2, 22] (*a.k.a.*, masked image modeling or BERT-style pre-training;

see Figure 1 (left)) or to predict images in auto-regressive language-modeling manner [6] (*a.k.a.*, autoregressive patch prediction or GPT-style pre-training; see Figure 1 (middle)). It is interesting to observe that on the NLP side, GPT models have shown to be powerful, while vision models have gravitated more towards BERT-style pre-training both with visual [6, 2] and multi-modal data [34, 45].

Motivated by this, in this paper, we adopt an autoregressive pre-training strategy and ask a number of important empirical questions about the use of such pre-training and what makes it effective. Specifically, (1) we ask what granularity (scale) and shape of tokens (patches, blobs) is most effective and how it affects the performance? (2) How best to serialize predictions? For example, previous approaches, such as image GPT [6], leveraged raster ordering. While such ordering is perhaps “optimal” from correlation and predictive/generative [37] points of view, we show that it is not optimal for general feature learning. We also explore (3) whether deterministic vs. stochastic tokenization and serialization are helpful. Finally, (4) we explore the effective interactions between the decoder and encoder layers; proposing a new ViT architecture that uses learned skip connections between encoder and decoder layers to improve performance.

Contributions. Overall, we make two core contributions. First, we propose a new pre-training strategy that leverages (randomly) sampled hierarchical segment cluster traversals to autoregressively train ViT models. This allows both short- and long-term spatial predictions, allowing distribution over easy and hard predictive tasks². We note that the effectiveness of single random segment inpainting was initially observed in [39], but is notably missing from most recent self-supervised strategies. Our pre-training strategy generalizes this observation and strategy to hierarchical and serialized predictions. Second, we propose a flexible ViT decoder that at each decoding layer learns to dynamically attend over different levels of features in the encoder. This in effect creates learned skip-connections, as compared to UNet [44] and others that require fixed connections in a symmetric encoder-decoder design, which further improve the performance.

Discussion. The above pre-training strategy, while empirically motivated, is also loosely modeled after human vision. Humans attend to the scene by a sequence of foveal observations, where an eye shifts over a series of fixation points; such motions are called *saccades*. Some saccades are long-range and voluntary, while others are local and involuntary (*a.k.a.*, microsaccades [43]). Our segments can be “viewed” as predictive foveal regions, and the hierarchical serialization of such regions as the combination of micro and macro saccades. The significant difference from human vision, is that in human vision saccades are purposeful and have been shown to be conditioned on the task [55]. In contrast, our pre-training such “saccadic” movements are randomly sampled. Learning a purposeful policy for hierarchical serialization of segments, for example, by Reinforcement Learn-

² This is, in part, motivated by [22] which observe that in BERT-style pre-training high amount of masking (as much as 75%), which corresponds to harder predictive tasks, leads to better feature learning.

ing techniques, would be an interesting future work that we plan to explore. However, this is a difficult task that is beyond the scope of this paper.

2 Related Work

Transformer-based Natural Language Modeling. In the field of natural language processing (NLP), two dominant self-supervised language modeling paradigms are Masked Language Modeling, such as BERT [15], and GPT-style autoregressive pre-training [3, 40, 41]. Given a sentence, BERT and its variants [29, 30] pre-train transformer encoders by predicting randomly masked out input words, referred to as *tokens*. Such frameworks model the bidirectional (contextual) dependencies between the visible tokens and the corrupted/masked tokens. GPT, which can be viewed as a special case of the transformer decoder, on the other hand, models the left-to-right natural order of languages. Recent advances in large-scale generative language modeling show powerful few-shot capabilities and are believed to be a promising path towards general machine intelligence. Permutation-based autoregressive model [54] was proposed to bridge the gap between autoregressive language modeling and masked autoencoding by maximizing the likelihood over all permutations of the factorization order. We take inspiration from GPT-style autoregressive pre-training in formulating our model, and focus on important aspects of mapping such strategy onto visual (ViT) models, where tokenization and serialization are not as well defined as in language.

Contrastive Image Learning. Contrastive methods [7, 23, 38, 47] and their negative-sample-free variants [10, 21, 26, 59] have emerged as dominant for unsupervised/self-supervised visual representation learning over the past 1–2 years. By building agreement among augmented versions of the input data, image features that are invariant of those perturbations can be learned. This method implicitly assumes a set of representational invariance (*e.g.*, color and spatial invariance). Once such representations are learned they are either used directly, or fine-tuned, to one or more downstream supervised tasks (*e.g.*, classification, detection, segmentation). When a downstream task violates the aforementioned invariance assumptions, they display poor transferability [52]. For example, the center-bias [9] and small-object feature suppression [8] have been observed in prior works. Masked image modeling & autoregressive image encoding, of which our method is an instance, tend to perform better in such circumstances [2, 22].

Masked Image Modeling. Early CNN-based masked image modeling, also known as image inpainting [16, 39, 57], has shown promising results but failed to become a predominant training paradigm, in part, due to its inferior performance with respect to large-scale supervised pre-training (*e.g.*, on ImageNet). The recent trend of incorporating transformers into vision architectures [4], or replacing CNN completely [17], by tokenizing images into a grid of non-overlapping patches, have enabled application of large scale NLP pretraining techniques in vision, *e.g.*, [2, 22, 51, 53]. Directly applying them to image pixels, however, leads

to inferior performance [6, 17]. To this end, BEiT [2] proposes to predict discrete masked image tokens. Masked Autoencoder (MAE) [22] suggests a 75% random masking ratio for image modeling; and SimMIM [53] studies different masking strategies for pretraining. MaskFeat [51] investigates five different reconstruction targets, and SplitMask [18] illustrates the ability of BEiT to train with small scale pre-training datasets. Our proposed RandSAC strategy, is related to masked image modeling, but is autoregressive in nature.

Autoregressive Image Encoding. Compared with BERT-style pre-training for vision transformers, GPT-like autoregressive models have been overlooked due to their complexity introduced by dense image pixels. In image GPT [6], images are limited to $64 \times 64 = 4096$ pixels. The 4096 pixels are tokenized and serialized in raster-order before feeding into a causal transformer. The quadratic time/space complexity of self-attention prevents the scaling of such approaches.

3 Random Segment with Autoregressive Coding

RandSAC learns representations through autoregressive image segment prediction. It partitions a tokenized image into random spatially coherent non-overlapping (hierarchical) segments, serializes them, and then autoregressively predicts tokens within these ordered segments. As a result, the token predictions between segments are sequential, while within a segment are parallel. This training strategy has four important components that we will explore:

- **Tokenization.** To use a transformer-based architecture, images need to be *tokenized*, *i.e.*, transformed into a set of basic image elements. For example, some approaches discreteize images [2, 6], while others patchify them [12, 17, 22, 53]. Tokenization strategy effects the spatial scale and number of tokens, which affects both performance and computation cost of the method.
- **Segment Partitioning.** After tokenizing the image, the tokens are grouped into spatially coherent segments. Those segments are autoregressively predicted following serialization order. The size and shape of segments and the way they are traversed can affect training and downstream performance.
- **Serialization Strategy.** Serialization strategy affects the traversal order of segments. In prior autoregressive modeling [6] raster-order is assumed. We show that stochastic (*i.e.*, randomized) serialization is much more effective.
- **Transformer Architecture.** In a GPT-style autoregressive model, the target sequence is identical to the shifted input sequence throughout training. However, for random segment prediction, the target sequence order varies for each sample. To enable this, we leverage a transformer decoder which takes as input position of each token and outputs its predicted representation conditioned on the transformer encoded context. In addition, we propose a novel trainable skip-connection layer for efficient decoding.

In the following section, the default option for model architecture is the vanilla masked transformer introduced in Section 4. We experiment with two different

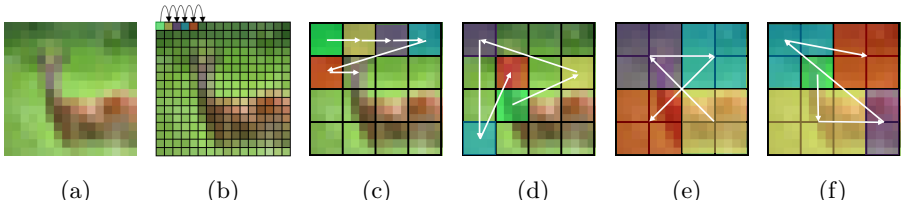


Fig. 2: **Illustration of Autoregressive Prediction Schemes.** Left-to-right: (a) original image from CIFAR 10; (b) raster-order pixel prediction; (c) raster-order patch prediction; (d) stochastic patch prediction; (e) stochastic square segment prediction ($M = 2$); (f) stochastic blob segment prediction ($K = 5$).

datasets, CIFAR10 [28] and ImageNet100 [47]. Evaluation protocols are introduced in Section 5, and implementation details are in the Supplemental. We use a simple mean square error (MSE) as our pixel reconstruction objective.

3.1 From Pixels to Segments

Tokenization. We start from raster-order serialization and compare two different tokenization strategies introduced by iGPT [6] and ViT [17]. Assume a dataset \mathcal{D} of images $\mathbf{X} \in \mathbb{R}^{H \times W \times C}$, where H, W, C are the height, width, and the number of channels of the image. We reshape each image into $N = HW/P^2$ patches, where P is the resolution of each patch. Tokens are obtained by linearly projecting the image patches $\mathbf{X} = \{\mathbf{x}_i\}_{i=1}^N$ and serialized in row-by-row fashion.

For pixel prediction experiment, we set $P = 1$, letting image patch size to be 1×1 pixels (see Figure 2 (b)). For ViT style patch prediction experiment, we split the 32×32 CIFAR10 image into $8 \times 8 = 64$ patches (see Figure 2 (c)), each patch consists of 4×4 pixels ($P = 4$). Note that for a fair comparison, we didn't strictly follow iGPT where they minimize the negative log-likelihood of the quantized RGB values. We simply adopt a mean squared error (MSE) between the predicted and target pixel values for all our experiments following [22]. Note that for visualizations in Figure 2 we use a downsampled CIFAR10 image.

The results for these two tokenization options are illustrated in Table 1 (additional scales are in Supplemental) under **pixel-raster** and **patch-raster** respectively in terms of linear probing and fine tuning accuracy (see Sec. 5.1 for definition of metrics). From the point of view of representation learning, patches are substantially better. Further, computationally, self-attention mechanism in a transformer uses $O(n^2)$ in both time and space with respect to the sequence length. Hence for pixel tokenization the complexity is $O((HW)^2)$. For patches the complexity is reduced to $O((HW/P^2)^2)$. In our CIFAR10 experiment, when $P = 4$, the complexity of training is lowered by a factor of $P^4 = 256$. Hence, **patches result in better tokenization**.

	pixel-raster	patch-raster
LIN(\uparrow)	41.70	55.53
FT(\uparrow)	59.35	78.67

Table 1: **Tokenization** on CIFAR10.

Stochastic Serialization. Randomized pretext tasks play an important role in a range of self-supervised learning algorithms. In NLP, for example, [54] improves fix-order autoregressive language models by allowing all possible permutations of the factorization order during training. For autoregressive ViT training of stochastic token serialization, we adopt a similar strategy by shuffling the token sequence for each image sample. Note that this does *not* mean that our prediction sequence is “orderless”. By moving from fixed raster-order prediction to randomized sequence prediction, keeping all else the same, we observe 20% improvement in linear evaluation and $\sim 10\%$ in fine-tuning (Table 2). **Stochastic serialization is clearly superior.**

3.2 Group Tokens into Segments

In this section, we introduce a concept of *segments*, which we define as groups (or clusters) of tokens. Effectively each segment forms an equivalency class within our serialized order, where tokens are encoded and decoded in parallel. Across segments, however, predictions are still strictly sequential. The motivation for introducing segments is two-fold. First, it allows us to reduce the overall autoregressive prediction steps. Second, it allows our autoregressive strategy to effectively leverage aspects of parallel, BERT-style, prediction locally. The autoregressive prediction steps can also be changed without introducing parallel prediction, simply by changing the patch size P . We show in Table 3 that a different patch size P does not lead to improved representation for a segment-free **patch-random** prediction task. In the following section, we experiment with two spatially coherent segment strategies (square and blob) and then look at the importance of this spatial coherence.

Square Segments. Once we have a grid of N patches of size $\frac{H}{P} \times \frac{W}{P}$, we reshape the tokens into a set of square segments $M \times M$, where the M denotes the size of the square. The segment count K of an image of $H \times W$ is thus defined by: $K = \frac{H \times W}{(P \times M)^2}$. For example, in our CIFAR10 experiment, an input image of size 32×32 is tokenized into a grid of 8×8 tokens, each of which is a 4×4 pixel patch. We set the square size $M = 2$, the tokens are then split into $(8/2)^2 = 16$ segments, which are shuffled randomly for autoregressive prediction as before. We list the representation quality with different square segment size (M) in Table 4. Since the grid size is

	patch-raster	patch-random
LIN(\uparrow)	55.53	75.53
FT(\uparrow)	78.67	87.52

Table 2: **Serialization** on CIFAR10.

	1 \times 1	2 \times 2	4 \times 4	8 \times 8	16 \times 16
LIN(\uparrow)	59.79	69.63	75.53	75.34	60.77
FT(\uparrow)	79.70	87.18	87.52	83.10	69.23

Table 3: **Patch-random** tokenization as a function of P on CIFAR10.

Square size M	1	2	4
LIN(\uparrow)	75.53	81.38	79.38
FT(\uparrow)	87.52	91.38	90.23

Table 4: **Square-random** serialization as a function of M on CIFAR10.

8×8 for CIFAR10, we chose square sizes $M = [1, 2, 4]$. Note that, when $M = 8$, there will be only one segment (e.g., $K = 1$) and no prediction can be made.

Blob Segments. We define blob segments as irregular elliptical segments defined by a sampled Mixture of Gaussians. To obtain K random blobs for a given image, we first sample K Gaussians with means sampled from $[\mu_k^{(x)}, \mu_k^{(y)}] \sim \mathcal{U}(-1.75, 1.75)$ and standard deviations from $[\sigma_k^{(x)}, \sigma_k^{(y)}] \sim \mathcal{U}(0.5, 1)$, where \mathcal{U} is a uniform distribution. Then we simply assign each token \mathbf{x}_i which is at a normalized position (x_i, y_i) in the range of $[-2, 2]$ (i.e., leftmost top token is at $(-2, -2)$, rightmost bottom token is at $(2, 2)$). The assignment is done as follows:

$$S(\mathbf{x}_i) = \arg \max_k \mathcal{N} \left(\begin{bmatrix} x_i \\ y_i \end{bmatrix} \mid \begin{bmatrix} \mu_k^{(x)} \\ \mu_k^{(y)} \end{bmatrix}, \begin{bmatrix} \sigma_k^{(x)} & 0 \\ 0 & \sigma_k^{(y)} \end{bmatrix}^2 \right). \quad (1)$$

S is a function that maps token to segments. The sampling for both square and blob are only used during segment predictive training and is disabled during evaluation. The computation cost for sampling is, comparatively, negligible. We illustrate the square and blob strategies in Figure 2 (e) and (f) respectively. Note that beyond the shape, blob segments allow for variability in size squares do not.

Analysis. As can be seen from Table 5, both square segments and blob segments surpass segment-free patch-based autoregression (see **square-random**

	patch-random	square-random	blob-random
LIN (\uparrow)	75.53	81.38	82.52
FT (\uparrow)	87.52	91.38	91.53

Table 5: **Segments** on CIFAR10.

and **blob-random** compared with **patch-random**). The blob segments and square segments behaves similarly. In addition, with blobs, we can easily modify the number of segments. However, with squares, the segment number is constrained by the token number. A grid of 8×8 tokens can either be segmented into 4×4 or 2×2 squares. A grid size of 13×13 can not be divided into any kind of squares. Blob segments on the other hand are more flexible and so we choose blobs for the remainder of our experiments.

Do segments need to be spatially coherent? The idea of a “segment” puts emphasis on the spatial coherence of the tokens. The upper part of Table 6 shows performance of feature representations with respect to number of blob segments K . In the bottom, we randomly shuffle all tokens so that tokens in any given “segment”

Table 6: **Segment Coherence.** Representation quality with different number of segments. Below we randomly permute the tokens such that the spatial coherence of segments is disrupted.

Segment K	3	5	7	9	11
LIN (\uparrow)	80.87	81.82	82.52	81.88	82.02
FT (\uparrow)	90.77	90.88	91.14	91.53	91.24
Shuffle	3	5	7	9	11
LIN (\uparrow)	76.73	77.73	76.69	78.59	76.99
FT (\uparrow)	89.63	89.75	89.22	90.00	89.15

Table 7: **Hierarchical Segment Prediction.** The number on top indicated the number of segments (*e.g.*, 3, 7), – no-hierarchy; the $7 \rightarrow 3$ indicates hierarchical variants with two levels – 7 segments that are then grouped into 3 partitions.

Segments	3	7	$7 \rightarrow 3$	5	11	$11 \rightarrow 5$	4	16	$16 \rightarrow 4$
CF10 Linear (\uparrow)	80.97	82.52	82.71	81.82	82.02	83.20	81.09	80.97	82.61
CF10 Fine-tune (\uparrow)	90.77	91.14	91.20	90.88	91.24	91.38	90.63	90.57	91.15
IN100 Linear (\uparrow)	56.26	63.36	64.54	62.10	65.86	65.76	60.62	64.50	64.92
IN100 Fine-tune (\uparrow)	81.34	84.36	84.48	83.75	85.16	85.94	83.07	86.06	86.18

no longer spatially coherent. We observe that feature learning deteriorates when segments are not spatially coherent. Note that segments without spatial coherence are still consistently better than **patch-random** from Table 5.

3.3 Hierarchical Segment Serialization

Images are hierarchical: a visual concept that occupies some region of an image can often be interpreted as a component of a greater whole [25] (*e.g.*, parts make up object, object scenes and so on). Such compositionality motivates hierarchical groupings. In our case of random segment serialization, we postulate that similar hierarchical traversal order, which adds certain degree of locality, may be useful.

In Figure 3 we illustrate this concept that we operationalize. An image is first partitioned into 7 (blob) segments, indicated by different colors and shades. We then group these 7 segments into 3 larger partitions following the same logic for segment generation. Different colors (*e.g.*, blue, purple, and green) represent these partition groups; segments that share partition differ in shade. Hierarchical serialization is obtained by randomly, and sequentially, predicting the segments inside of each partition group (shown by the black arrows), and then jumping to another partition group at random. Note that the segment-level (local) and partition-level (global) serializations are both random. This idea can be extended to deeper hierarchies, with the depth of the hierarchy and grouping chosen based on the resolution and nature of the dataset.

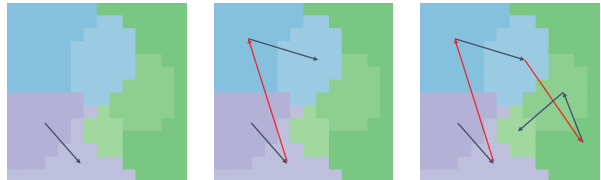


Fig. 3: **Hierarchical Segment Serialization.** We partition an image into a hierarchy of segments. Autoregressive prediction is done by following a traversal of randomly generated hierarchical partitions.

Experimental results that compare flat segments to two-level hierarchy are illustrated in Table 7. We perform these experiments on both CIFAR10 and ImageNet100 datasets. Our experiments show that hierarchical serialization and prediction consistently outperform the non-hierarchical counterparts.

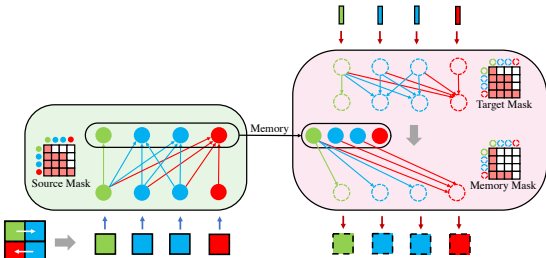


Fig. 4: Attention-masking for Autoregressive Segment Prediction. For an image converted into a sequence of patches, we adopt a masked encoder-decoder transformer [49] for autoregressive segment prediction. In the encoder, causal *source mask* enables a given segment to only attend over preceding segments and the tokens within itself. The decoder, given position of tokens as input, predicts tokens within each segment conditioned on encoded previous segments (enabled by the *memory mask*).

4 Architecture

Image GPT [6] performs autoregressive prediction by shifting the source sequence one pixel to the right. Since the raster ordering of iGPT is fixed for all samples throughout training, the position for the next target token is implicitly modeled by the transformer. In contrast, in our autoregressive segment modeling framework, the next token depends on the serialization strategy, thus can vary from sample to sample during training. Moreover, when predicting the next segment, the tokens within each segment should be predicted jointly (in parallel). This requires lateral pathways that allow communication within target segments. To tackle the aforementioned problems, we propose to utilize the transformer decoder.

4.1 Masked Transformer for Segment Prediction

A standard transformer has an encoder-decoder structure [49]. It was originally designed for sequence-to-sequence modeling. The encoder of a transformer maps a list of tokens $\mathbf{X} = (\mathbf{x}_1, \dots, \mathbf{x}_n)$ to a sequence of hidden representation $\mathbf{Z} = (\mathbf{z}_1, \dots, \mathbf{z}_n)$, also known as the *memory*. Given \mathbf{X} and source sequence $\mathbf{X}_{src} = (\mathbf{x}_1, \dots, \mathbf{x}_{n-1})$, during training, the decoder masks the internal attention matrix with a causal mask and predicts the target sequence $\mathbf{X}_{tgt} = (\mathbf{x}_2, \dots, \mathbf{x}_n)$ autoregressively. Each layer of the transformer encoder has two sub-layers: multi-head self-attention and a fully connected feed-forward network; both have residual connections. The decoder layer has a third attention sub-layer, which performs multi-head attention from the hidden representation \mathbf{Z} to the target representation \mathbf{X}_{tgt} . We leverage attention masking to achieve autoregressive segment prediction using this framework; we discuss this in detail next.

Autoregressive Segment Encoder. Figure 4 shows our transformer encoder block and a decoder block. We leave out the fully connected layer and residual connections for simplicity and only show the attentions. In this visualization, an

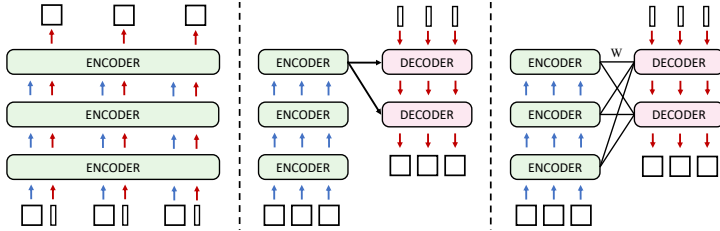


Fig. 5: **Candidate architectures for autoregressive segment prediction:** Left: Two-stream Transformer [54]. Middle: Masked Transformer. Right: proposed Masked Transformer with Trainable Skip Connections.

image is divided into four patches/tokens. These four patches are then grouped into three segments denoted by colors: green, blue, and red. The random segment serialization order is green \rightarrow blue \rightarrow red. One layer of transformer encoder is illustrated on the left in light green. Serialized four patches/tokens with added fixed sine-cosine positional encoding are the input to the encoder. The encoder attention is masked following the serialized segment order: segments can attend to themselves and preceding segments only. They are restricted from looking at future segments using the, illustrated, *source mask*.

Autoregressive Segment Decoder. The input for the transformer decoder, illustrated on the right of Figure 4 in pink, is a set of fixed positional encodings to guide the reconstruction of target segments and tokens. The self-attention layer of the decoder is masked the same way as the encoder for autoregressive segment decoding. This layer enables co-attention over preceding and current segment for context. We mask the second multi-head attention layer, that attends over memory (*i.e.*, encoder output), differently. To disallow “cheating” we, in addition, mask encoding of tokens that are part of the segment being predicted. Not doing so would allow the segment to look at its own encoding, instead of leveraging autoregressive predictive mechanism, which would clearly be problematic. Lastly, since the first segment in the sequence does not have a preceding segment, we allow it to attend to its own encoding.

Evaluation. During linear evaluation and fine-tuning, both the attention masks and decoder are removed, and the encoder is used as feature extractor for the downstream supervised classification.

4.2 Trainable Skip Connections

The original transformer decoder layer can only attend to the same encoder output, often from the last layer of the encoder. In contrast, CNN encoder-decoder architectures are often symmetric with skip connections between encoder and decoder layers, *e.g.*, UNet [44]. We hypothesize that in our asymmetrical design, skip-connections between transformer encoder and decoder can similarly be beneficial. To enable such skip connections, we propose a trainable skip connection module that learns how to assign encoder memory to the decoder layers.

	CIFAR10				ImageNet100			
	Enc	Dec	LIN (\uparrow)	FT (\uparrow)	Enc	Dec	LIN (\uparrow)	FT (\uparrow)
Two-stream	7M	0M	84.4	91.5	30M	0M	62.4	84.6
Transformer	5M	2M	88.0	93.6	21M	9M	65.8	85.9
Transformer-skip	5M	2M	89.5	94.4	21M	9M	70.7	87.3

Table 8: **Performance of Architectures for RandSAC.** See text for details.

A transformer with L_{enc} encoder layers and L_{dec} decoder layers processes input \mathbf{X} into L_{enc} hidden representations $\mathbf{H}_{enc}^l = (\mathbf{h}_1^l, \dots, \mathbf{h}_n^l)$. In traditional masked transformer, decoder memory is set to $\mathbf{Z}^l = \mathbf{H}_{enc}^{L_{enc}}$ for each layer l of the decoder. Instead, we introduce a linear attention layer that allows each decoder layer to attend over encoding hidden representations. In other words, we learn a linear layer with parameters $\mathbf{W} \in \mathcal{R}^{L_{enc} \times L_{dec}}$, such that: $\mathbf{Z}^l = \sum_{k=1}^{L_{enc}} \mathbf{W}_{l,k} \mathbf{H}_{enc}^k$. Note, the linearly combined memory cells are conditioned on, and different, for each individual decoder layer. To evaluate the effectiveness of the proposed Masked Transformer and trainable skip connection layer for segment prediction, we compare three architectures:

Two-stream Transformer. This design was proposed in [54] for permutation-based language modeling. It enables randomized target predictions by leveraging a two-stream attention layer: the *content* stream encodes the full contextual information, and the *query* stream, which only has access to the previous content, is designed to make current predictions. We apply this architecture for our segment prediction by setting the *content mask* with our “source mask” and *query mask* with our “memory mask”. Model weights for both content stream and query stream are shared (see Figure 5 (left) for illustration of design).

Masked Transformer. For masked transformer we utilize architecture described in Section 4.1 and illustrated in Figure 4; also in Figure 5 (middle). Compared with the Two-stream Transformer above, this design enables communication among jointly predicted tokens within a segment. Also, compared with Two-stream Transformer, weights for encoding and decoding the segment content are decoupled in the Masked Transformer.

Masked Transformer with Trainable Skip Connections. A Masked Transformer only decodes based on the (last layer) encoder output. A trainable skip connection layer we introduce dynamically allocates memory assignments between intermediate layers of transformer-encoder-decoder (see Figure 5 (right)). As can be seen from the results in Table 8, this variant does outperform the two competitors on both CIFAR10 and ImageNet100 datasets.

5 Experiments

We test RandSAC on two drastically different settings: low-data and ImageNet-1K pre-training. We evaluate the classification performance of our pretrained

backbone with linear probing and fine-tuning. We also test the transfer learning ability of our ImageNet pretrained model with semantic segmentation on ADE20K.

Implementation Details. We adopt minimal data augmentation strategy following [22]: resize cropping with scale range of $[0.2, 1.0]$ and aspect ratio is sampled within range $[\frac{3}{4}, \frac{4}{3}]$, followed by a 50% chance random horizontal flipping. We do *not* use color jittering, path dropping, or gradient clip in pretraining. We use AdamW as optimizer and pretrain RandSAC for 1600 epochs. We use a linear *lr* scaling rule [20] that scales the *base_lr* by *batchsize*/256. The *lr* is scheduled to warm-up from 0 to *base_lr*, then decayed following a cosine-decay rule [32]. For both benchmarks, we use the *normalized pixel loss* introduced from [22] as our patch regression target. Our loss function computes the mean squared error (MSE) between the patch-normalized reconstruction and original image pixels.

Low-data Pretraining. Vision transformers are known to be “data hungry” [17] and require a large dataset and a series of data augmentations to pretrain [48]. To experiment in such a challenging setting, we evaluate our method on small-scale datasets with minimal augmentation. We train a “blob” RandSAC model using hierarchy 11 \rightarrow 5. We pre-train ViT-Small on **CIFAR10** and **CIFAR100** [28]. Both datasets are small-scale image datasets containing 60000 32×32 images that belong to 10 and 100 categories, respectively. The ViT-Small has 12 layers. Each layer has 384 dimensions and 6 self-attention heads. We chose patch size 4×4 and split the 32×32 images into 8×8 tokens. For segment decoding, we use a 6 transformer decoder layer. The attention-head and feature dimension of the decoder are the same as the encoder. We also set the decoder for MAE [22] to have the same depth, attention head, and dimension as ours. The batch size is 512 and we set weight decay to be 0.05, $\beta_1 = 0.9$ and $\beta_2 = 0.999$. $base_lr = 1e^{-3}$ and the warm-up is 10 epochs. More details are in Supplemental.

Pretraining on ImageNet-1K. ImageNet ILSVRC-2012 [14] is a popular large scale image dataset with 1.28 million images and 1000 categories. We pretrain blob-RandSAC with hierarchy 11 \rightarrow 7 \rightarrow 3 using ViT-Base [17] on ImageNet-1K following [2, 22]. ViT-Base model has 12 blocks with each block having dimension 768 and 12 heads. We chose a 4 layer decoder with dimension 512 and 16 heads. The batchsize is 4096. The weight decay, β_1 and β_2 for AdamW is set to be 0.05, 0.9 and 0.95 respectively. We use a 40 epoch warm-up and set the $base_lr = 1.5e^{-4}$. More details are in Supplemental.

5.1 Evaluation protocols

Linear Probing. This measure is widely used for quantifying the quality of representation learning. It learns a linear classifier on top of the frozen feature of a pretrained encoder to classify the object-level classification labels. Then performance is evaluated using the val/test set. Note that the dimension of the feature that the classifier is trained on, may influence the eventual accuracy readout [5]. A longer feature vector is likely to produce a better linear result.

Prior works such as [5] concatenate the feature vectors from the last 4 ViT blocks and [6] use feature vectors up to 15360 dimensions for evaluation. We, however, use only the last encoder averaged feature output following [22, 11] (*i.e.*, 384 dimensions for ViT-S and 768 dimensions for ViT-B). The linear classifier is trained for 90 epochs. Detailed hyper-parameter settings are in Supplemental.

End-to-end Fine-tuning. A recent study [9] shows that linear evaluation favors those methods with a *center-bias* such as contrastive learning. To complement linear probing, we also include 100-epoch fine-tuning evaluation. In fine-tuning, all parameters are optimized for classification. The fine-tuning recipe follows the common practice of supervised ViT training. Details in Supplemental.

5.2 Results

Table 9 shows low-data classification performance for contrastive pretraining (DINO [5]), masked image encoding (MAE [22]) and our segment autoregressive coding (RandSAC). The MAE and DINO are pretrained using their official implementations. For MAE we use a 75% masking ratio as suggested in their paper. All models are pretrained for 1600 epochs and evaluated with both 90-epoch linear probing (LIN) and 100-epoch fine-tuning (FT). Under the low data benchmark, RandSAC outperforms other non-autoregressive algorithms and direct supervised training, by a large margin. We postulate that the superior performance of RandSAC comes from randomized segment prediction pretext task. The autoregressive coding objective that we propose, which is to traverse a hierarchy of randomly serialized visual segments(components), diversifies the small dataset, and serves as a sort of data augmentation.

Table 10 shows ImageNet pretraining result. We compare RandSAC with contrastive transformer training approaches (DINO [5] & MoCo v3 [11]), masked image encoding (BEIT [2] & MAE [22]), and our autoregressive counterpart iGPT [6]. We note, that due to limited access to computation we were only able to run RandSAC once, without any parameter tuning. Nether the less, RandSAC outperforms all predictive (non-contrastive methods) in linear probing, despite having 36% fewer parameters in the decoder as compared to MAE [22]. Our experiments strongly suggest that with some parameter tuning, results can be further improved.

Contrastive models do tend to perform better, but also differ in pre-training. For example, contrastive methods require two global crops of the input image while other methods only process one crop; DINO uses **10** local crops. In addition, linear probing for DINO and iGPT is evaluated using the last 4 and 5 transformer blocks, respectively, while MoCo v3, MAE, and RandSAC only

Model	CIFAR10		CIFAR100	
	LIN	FT	LIN	FT
Supervised	91.3		64.13	
DINO [5]	89.0	94.4	65.78	76.3
MAE [22]	87.3	95.9	54.0	81.1
RandSAC	93.9	96.9	67.9	79.6

Table 9: Low-data pre-training with CIFAR10 and CIFAR100

Model	Backbone	Encoder	Decoder	Linear	Fine-tune
Supervised	ViT-Base	86M	0M	76.4	76.4
DINO [5]	ViT-Base	85M	0M	78.2	82.8
MoCo v3 [11]	ViT-Base	86M	0M	76.7	83.2
BEiT [2]	ViT-Base	86M	0M	None	83.2
BEiT [2]	ViT-Large	304M	0M	52.1	85.2
MAE [22]	ViT-Base	86M	25M	68.0	83.6
IGPT [6]	IGPT-S	76M	0M	41.9	None
IGPT [6]	IGPT-M	455M	0M	54.5	None
IGPT [6]	IGPT-L	1362M	0M	65.2	None
RandSAC	ViT-Base	86M	16M	68.3	83.0

Table 10: ImageNet experiment.

evaluate the last block output. A longer feature vector tends to result in better linear probing accuracy [5, 6]. Lastly, it is worth mentioning that RandSAC can be easily combined with contrastive objectives in the future.

Semantic segmentation on ADE20K. We take our pre-trained backbone as initialization and end-to-end fine-tune with UpperNet framework on ADE20k to evaluate the performance of our pre-trained model on downstream task, semantic segmentation.

We follow the same setting of BeiT [2]; more details are given in Supplemental. We compare our pre-training with supervised pre-training, MoCo, DINO, and BeiT in Table 11. Our pre-training outperform DeiT, MoCo, DINO, BeiT by 0.3, 0.1, 0.1 and 0.8 respectively.

Table 11: Semantic segmentation on ADE20K.

Method	Crops	Super.	Self-super.	mIoU
DeiT [48]	1	✓	✗	47.0
MoCo v3 [11]	2	✗	✓	47.2
DINO [5]	2+10	✗	✓	47.2
BEiT [2]	1	✗	✓	46.5
Ours	1	✗	✓	47.3

6 Conclusion

We present a new self-supervised pre-training strategy we call RandSAC. In doing so, we also study and provide general insights into ViT pre-training (*e.g.*, tokenization, segmentation, and serialization). We found randomized serialization of hierarchical image segments significantly improves autoregressive pre-training of vision transformers. In addition, we propose a new design for the transformer decoder, which facilitates improved performance. We show evidence that such a proposed task and model could be the key to developing a powerful GPT-like model for visual representation learning.

7 Acknowledgements

This work was funded, in part, by the Vector Institute for AI, Canada CIFAR AI Chair, NSERC CRC, and an NSERC DG and Discovery Accelerator Grants. Resources used in preparing this research were provided, in part, by the Province of Ontario, the Government of Canada through CIFAR, and companies sponsoring the Vector Institute <https://vectorinstitute.ai/partners/>. Additional hardware support was provided by John R. Evans Leaders Fund CFI grant and Compute Canada under the Resource Allocation Competition award. Finally, we would like to sincerely thank Muchen Li for valuable feedback and discussions.

References

1. Antol, S., Agrawal, A., Lu, J., Mitchell, M., Batra, D., Zitnick, C.L., Parikh, D.: Vqa: Visual question answering. In: IEEE International Conference on Computer Vision (ICCV). pp. 2425–2433 (2015) [1](#)
2. Bao, H., Dong, L., Wei, F.: BEiT: Bert pre-training of image transformers. International Conference on Learning Representations (ICLR) (2022) [2](#), [3](#), [4](#), [5](#), [13](#), [14](#), [15](#), [21](#)
3. Brown, T., Mann, B., Ryder, N., Subbiah, M., Kaplan, J.D., Dhariwal, P., Neelakantan, A., Shyam, P., Sastry, G., Askell, A., et al.: Language models are few-shot learners. Advances in Neural Information Processing Systems (NeurIPS) **33**, 1877–1901 (2020) [2](#), [4](#)
4. Carion, N., Massa, F., Synnaeve, G., Usunier, N., Kirillov, A., Zagoruyko, S.: End-to-end object detection with transformers. European Conference on Computer Vision (ECCV) (2020) [4](#), [20](#)
5. Caron, M., Touvron, H., Misra, I., Jégou, H., Mairal, J., Bojanowski, P., Joulin, A.: Emerging properties in self-supervised vision transformers. In: IEEE/CVF International Conference on Computer Vision (ICCV). pp. 9650–9660 (2021) [13](#), [14](#), [15](#)
6. Chen, M., Radford, A., Child, R., Wu, J., Jun, H., Luan, D., Sutskever, I.: Generative pretraining from pixels. In: International Conference on Machine Learning (ICML). pp. 1691–1703 (2020) [3](#), [5](#), [6](#), [10](#), [14](#), [15](#), [21](#), [22](#)
7. Chen, T., Kornblith, S., Norouzi, M., Hinton, G.E.: A simple framework for contrastive learning of visual representations. ArXiv [abs/2002.05709](#) (2020) [4](#)
8. Chen, T., Luo, C., Li, L.: Intriguing properties of contrastive losses. Advances in Neural Information Processing Systems (NeurIPS) **34** (2021) [2](#), [4](#)
9. Chen, X., Ding, M., Wang, X., Xin, Y., Mo, S., Wang, Y., Han, S., Luo, P., Zeng, G., Wang, J.: Context autoencoder for self-supervised representation learning. arXiv preprint arXiv:2202.03026 (2022) [2](#), [4](#), [14](#)
10. Chen, X., He, K.: Exploring simple siamese representation learning. 2021 IEEE/CVF Conference on Computer Vision and Pattern Recognition (CVPR) pp. 15745–15753 (2021) [4](#)
11. Chen, X., Xie, S., He, K.: An empirical study of training self-supervised vision transformers. IEEE/CVF International Conference on Computer Vision (ICCV) (2021) [14](#), [15](#)
12. Cordonnier, J.B., Loukas, A., Jaggi, M.: On the relationship between self-attention and convolutional layers. International Conference on Learning Representations (ICLR) (2020) [5](#)

13. Cubuk, E.D., Zoph, B., Shlens, J., Le, Q.V.: Randaugment: Practical automated data augmentation with a reduced search space. In: IEEE Conference on Computer Vision and Pattern Recognition Workshops (2020) [22](#)
14. Deng, J., Dong, W., Socher, R., Li, L.J., Li, K., Fei-Fei, L.: Imagenet: A large-scale hierarchical image database. In: IEEE Conference on Computer Vision and Pattern Recognition (CVPR). pp. 248–255. Ieee (2009) [13](#)
15. Devlin, J., Chang, M.W., Lee, K., Toutanova, K.: Bert: Pre-training of deep bidirectional transformers for language understanding. arXiv preprint arXiv:1810.04805 (2018) [2, 4](#)
16. Doersch, C., Gupta, A., Efros, A.A.: Unsupervised visual representation learning by context prediction. In: IEEE/CVF International Conference on Computer Vision (ICCV) (2015) [2, 4](#)
17. Dosovitskiy, A., Beyer, L., Kolesnikov, A., Weissenborn, D., Zhai, X., Unterthiner, T., Dehghani, M., Minderer, M., Heigold, G., Gelly, S., Uszkoreit, J., Houlsby, N.: An image is worth 16x16 words: Transformers for image recognition at scale. International Conference on Learning Representations (ICLR) (2021) [2, 4, 5, 6, 13, 20, 21](#)
18. El-Nouby, A., Izacard, G., Touvron, H., Laptev, I., Jégou, H., Grave, E.: Are large-scale datasets necessary for self-supervised pre-training? ArXiv [abs/2112.10740](#) (2021) [5](#)
19. Glorot, X., Bengio, Y.: Understanding the difficulty of training deep feedforward neural networks. In: AISTATS (2010) [20](#)
20. Goyal, P., Dollár, P., Girshick, R.B., Noordhuis, P., Wesolowski, L., Kyrola, A., Tulloch, A., Jia, Y., He, K.: Accurate, large minibatch sgd: Training imagenet in 1 hour. ArXiv [abs/1706.02677](#) (2017) [13](#)
21. Grill, J.B., Strub, F., Altch'e, F., Tallec, C., Richemond, P.H., Buchatskaya, E., Doersch, C., Pires, B.Á., Guo, Z.D., Azar, M.G., Piot, B., Kavukcuoglu, K., Munos, R., Valko, M.: Bootstrap your own latent: A new approach to self-supervised learning. Conference on Neural Information Processing Systems (NeurIPS) (2020) [4](#)
22. He, K., Chen, X., Xie, S., Li, Y., Dollár, P., Girshick, R.: Masked autoencoders are scalable vision learners. arXiv preprint arXiv:2111.06377 (2021) [2, 3, 4, 5, 6, 13, 14, 15, 20, 21](#)
23. He, K., Fan, H., Wu, Y., Xie, S., Girshick, R.B.: Momentum contrast for unsupervised visual representation learning. 2020 IEEE/CVF Conference on Computer Vision and Pattern Recognition (CVPR) pp. 9726–9735 (2020) [4](#)
24. He, K., Gkioxari, G., Dollár, P., Girshick, R.: Mask r-cnn. In: IEEE International Conference on Computer Vision (ICCV). pp. 2961–2969 (2017) [1](#)
25. Hinton, G.E.: How to represent part-whole hierarchies in a neural network. ArXiv [abs/2102.12627](#) (2021) [9](#)
26. Hua, T., Wang, W., Xue, Z., Wang, Y., Ren, S., Zhao, H.: On feature decorrelation in self-supervised learning. ArXiv [abs/2105.00470](#) (2021) [4](#)
27. Huang, G., Sun, Y., Liu, Z., Sedra, D., Weinberger, K.Q.: Deep networks with stochastic depth (2016) [22](#)
28. Krizhevsky, A.: Learning multiple layers of features from tiny images (2009) [6, 13](#)
29. Lan, Z., Chen, M., Goodman, S., Gimpel, K., Sharma, P., Soricut, R.: Albert: A lite bert for self-supervised learning of language representations. ArXiv [abs/1909.11942](#) (2020) [4](#)
30. Liu, Y., Ott, M., Goyal, N., Du, J., Joshi, M., Chen, D., Levy, O., Lewis, M., Zettlemoyer, L., Stoyanov, V.: Roberta: A robustly optimized bert pretraining approach. ArXiv [abs/1907.11692](#) (2019) [4](#)

31. Liu, Z., Lin, Y., Cao1, Y., Hu1, H., Wei, Y., Zhang, Z., Lin, S., Guo, B.: Swin transformer: Hierarchical vision transformer using shifted windows. In: IEEE/CVF International Conference on Computer Vision (ICCV) (2021) [2](#)
32. Loshchilov, I., Hutter, F.: Sgdr: Stochastic gradient descent with warm restarts. arXiv preprint arXiv:1608.03983 (2016) [13](#), [20](#), [21](#), [22](#)
33. Loshchilov, I., Hutter, F.: Decoupled weight decay regularization. International Conference on Learning Representations (ICLR) (2019) [20](#), [21](#)
34. Lu, J., Batra, D., Parikh, D., Lee, S.: VilBERT: Pretraining task-agnostic visiolinguistic representations for vision-and-language tasks. In: Conference on Neural Information Processing Systems (NeurIPS) (2019) [3](#)
35. Mayo, B., Hazan, T., Tal, A.: Visual navigation with spatial attention. In: IEEE/CVF Conference on Computer Vision and Pattern Recognition (CVPR). pp. 16898–16907 (2021) [1](#)
36. Noroozi, M., Favaro, P.: Unsupervised learning of visual representations by solving jigsaw puzzles. In: European Conference on Computer Vision (ECCV). pp. 69–84 (2016) [2](#)
37. van den Oord, A., Kalchbrenner, N., Kavukcuoglu, K.: Pixel recurrent neural networks. In: International Conference on Machine Learning (ICML) (2016) [3](#)
38. van den Oord, A., Li, Y., Vinyals, O.: Representation learning with contrastive predictive coding. ArXiv [abs/1807.03748](#) (2018) [4](#)
39. Pathak, D., Krahenbuhl, P., Donahue, J., Darrell, T., Efros, A.A.: Context encoders: Feature learning by inpainting. In: IEEE/CVF Conference on Computer Vision and Pattern Recognition (CVPR) (2016) [2](#), [3](#), [4](#)
40. Radford, A., Narasimhan, K.: Improving language understanding by generative pre-training (2018) [4](#)
41. Radford, A., Wu, J., Child, R., Luan, D., Amodei, D., Sutskever, I.: Language models are unsupervised multitask learners (2019) [4](#)
42. Redmon, J., Divvala, S., Girshick, R., Farhadi, A.: You only look once: Unified, real-time object detection. In: IEEE Conference on Computer Vision and Pattern Recognition (CVPR). pp. 779–788 (2016) [1](#)
43. Rolfs, M.: Microsaccades: small steps on a long way. Vision research **49**(20), 2415–2441 (2009) [3](#)
44. Ronneberger, O., Fischer, P., Brox, T.: U-Net: Convolutional networks for biomedical image segmentation. In: Medical Image Computing and Computer-Assisted Intervention (MICCAI). pp. 234–241 (2015) [3](#), [11](#)
45. Su, W., Zhu, X., Cao, Y., Li, B., Lu, L., Wei, F., Dai, J.: VL-BERT: Pre-training of generic visual-linguistic representations. In: International Conference on Learning Representations (ICLR) (2020) [3](#)
46. Szegedy, C., Vanhoucke, V., Ioffe, S., Shlens, J., Wojna, Z.: Rethinking the inception architecture for computer vision. In: IEEE Conference on Computer Vision and Pattern Recognition(CVPR) (2016) [22](#)
47. Tian, Y., Krishnan, D., Isola, P.: Contrastive multiview coding. In: European Conference on Computer Vision (ECCV) (2020) [4](#), [6](#), [20](#)
48. Touvron, H., Cord, M., Douze, M., Massa, F., Sablayrolles, A., Jégou, H.: Training data-efficient image transformers & distillation through attention. In: International Conference on Machine Learning (ICML). pp. 10347–10357 (2021) [13](#), [15](#)
49. Vaswani, A., Shazeer, N., Parmar, N., Uszkoreit, J., Jones, L., Gomez, A.N., Kaiser, L., Polosukhin, I.: Attention is all you need. Advances in Neural Information Processing Systems (NeurIPS) **30** (2017) [10](#)

50. Vincent, P., Larochelle, H., Bengio, Y., Manzagol, P.A.: Extracting and composing robust features with denoising autoencoders. In: International Conference on Machine Learning (ICML). pp. 1096–1103 (2008) [2](#)
51. Wei, C., Fan, H., Xie, S., Wu, C., Yuille, A.L., Feichtenhofer, C.: Masked feature prediction for self-supervised visual pre-training. ArXiv [abs/2112.09133](#) (2021) [4, 5](#)
52. Xiao, T., Wang, X., Efros, A.A., Darrell, T.: What should not be contrastive in contrastive learning. International Conference on Learning Representations (ICLR) (2021) [4](#)
53. Xie, Z., Zhang, Z., Cao, Y., Lin, Y., Bao, J., Yao, Z., Dai, Q., Hu, H.: SimMIM: A simple framework for masked image modeling. IEEE/CVF Conference on Computer Vision and Pattern Recognition (CVPR) (2022) [4, 5](#)
54. Yang, Z., Dai, Z., Yang, Y., Carbonell, J.G., Salakhutdinov, R., Le, Q.V.: Xlnet: Generalized autoregressive pretraining for language understanding. In: Conference on Neural Information Processing Systems (NeurIPS) (2019) [4, 7, 11, 12](#)
55. Yarbus, A.L.: Eye Movements and Vision. Springer (1967) [3](#)
56. You, Y., Gitman, I., Ginsburg, B.: Large batch training of convolutional networks. arXiv: Computer Vision and Pattern Recognition (2017) [22](#)
57. Yu, J., Lin, Z.L., Yang, J., Shen, X., Lu, X., Huang, T.S.: Generative image inpainting with contextual attention. IEEE/CVF Conference on Computer Vision and Pattern Recognition (CVPR) pp. 5505–5514 (2018) [4](#)
58. Yun, S., Han, D., Oh, S.J., Chun, S., Choe, J., Yoo, Y.J.: Cutmix: Regularization strategy to train strong classifiers with localizable features. IEEE/CVF International Conference on Computer Vision (ICCV) (2019) [22](#)
59. Zbontar, J., Jing, L., Misra, I., LeCun, Y., Deny, S.: Barlow twins: Self-supervised learning via redundancy reduction. In: International Conference on Machine Learning (ICML) (2021) [4](#)
60. Zhang, H., Cisse, M., Dauphin, Y.N., Lopez-Paz, D.: mixup: Beyond empirical risk minimization. International Conference on Learning Representations (ICLR) (2017) [22](#)
61. Zhang, R., Isola, P., Efros, A.A.: Colorful image colorization. In: European Conference on Computer Vision (ECCV) (2016) [2](#)

A Details for Section 3

A.1 Pre-training settings for CIFAR10 and ImageNet100

The following is the experiment configurations for CIFAR10 and ImageNet100 from Section 3 of the main paper. Details for end-to-end fine-tuning and linear probing are the same with ImageNet-1K.

CIFAR10 Experiments. The default setting is illustrated in Table 13. In this experiment, by default, we train a “blob” RandSAC model using hierarchy $11 \rightarrow 5$ (unless otherwise specified in Table 6). We pre-train ViT-Tiny encoder on CIFAR10. The ViT-Tiny has 12 layers. Each layer has 192 dimensions and 3 self-attention heads. We chose patch size 4×4 and split the 32×32 images into 8×8 tokens. For segment decoding, we use a 3 transformer decoder layers following the same configuration for encoder.

config	value
optimizer	AdamW [33]
base_lr	0.001
weight decay	0.05
β_1, β_2	0.9, 0.999 [4]
batch size	512
learning rate schedule	cosine decay [32]
warmup epochs	10
training epochs	800 (Table 1-6) 1600 (Table 7)
augmentation	RandomResizedCrop
norm_pixel_loss	False (Table 1-6) True [22] (Table 7)

Table 12: **CIFAR10 Pre-training setting.**

ImageNet100 Experiments. These experiments are included in Table 6-7 to complement CIFAR10 experiments. Similar to CIFAR10 experiments, we train a “blob” RandSAC model using default hierarchy $11 \rightarrow 5$. We pre-train ViT-Small encoder on ImageNet100 [47]. The ViT-Small backbone has 12 layers. Each layer has 384 dimensions and 6 self-attention heads. We chose patch size 16×16 following [17] and split the 224×224 images into 14×14 tokens. For segment decoding, we use a 4 layer transformer decoder and double the attention heads while keeping all other configurations the same from the ViT-Small encoder.

B Details for Section 4

B.1 ImageNet-1K Pre-training Setting

We follow closely the setup in [22] to pretrain ImageNet-1K. We use xavier_uniform [19] to initialize all Transformer blocks, following ViT’s official code [17].

config	value
optimizer	AdamW [33]
base_lr	1.5e-4 [22]
weight decay	0.05
β_1, β_2	0.9, 0.95 [6]
batch size	4096
learning rate schedule	cosine decay [32]
warmup epochs	40
training epochs	800
augmentation	RandomResizedCrop
norm_pixel_loss	True

Table 13: **ImageNet100 Pre-training setting.**

config	value
optimizer	AdamW [33]
base_lr	1.5e-4
weight decay	0.05
β_1, β_2	0.9, 0.95 [6]
batch size	4096
learning rate schedule	cosine decay [32]
warmup epochs	40
training epochs	1600
augmentation	RandomResizedCrop
norm_pixel_loss	True

Table 14: **ImageNet-1K pre-training setting.**

B.2 Evaluation Configurations

Different from ViT [17], where an additional class token is required for classification, we directly use the averaged pooled feature out of the encoder for both fine-tuning and linear probing. The hyper-parameters for both end-to-end fine-tuning and linear probing from Table 15 and Table 16 are used for all experiments of this paper.

C Implementation details of Semantic Segmentation

We end-to-end fine-tune our pre-trained ViT encoder with UpperNet framework on ADE20k to evaluate the performance on downstream task, semantic segmentation. We follow the same setting of BeiT [2]. We take AdamW as the optimizer and set the batch size to 16, the layer-wise decay rate to 0.65, the input resolution to 512×512 , fine-tuning iterations are set to 160K steps. During evaluation, we do not take multi-scale testing strategy in our experiment.

config	value
optimizer	AdamW
base_lr	5e-4
weight decay	0.05
β_1, β_2	0.9, 0.999 [6]
layer-wise lr decay	0.65
batch size	1024
learning rate schedule	cosine decay [32]
warmup epochs	5
training epochs	100
augmentation	RandAug (9, 0.5) [13]
label smoothing [46]	0.1
mixup [60]	0.8
cutmix [58]	1.0
drop path [27]	0.1

Table 15: End-to-end fine-tuning setting.

config	value
optimizer	LARS [56]
base_lr	0.1
weight decay	0
momentum	0.9
batch size	16384
learning rate schedule	cosine decay
warmup epochs	10
training epochs	90
augmentation	RandomResizedCrop

Table 16: Linear probing setting.

D Code and Reproducibility

We will release code and all pre-trained models upon acceptance of the paper.

E Visualization of Tokenization and Serialization

We visualize different tokenization and serialization schemes discussed in the main paper in the video file included as part of the supplemental materials.